Chinese Chemical Letters 34 (2023) 108034

Contents lists available at ScienceDirect

Chinese Chemical Letters

journal homepage: www.elsevier.com/locate/cclet

Self-supported ultrathin Co_3O_4 nanoarray enabling efficient paired electrolysis of 5-hydroxymethylfurfural for simultaneous dihydroxymethylfuran (DHMF) and furandicarboxylic acid (FDCA) production

Xiaoqiang Pan, Shuchuan Mei, Wu-Jun Liu*

CAS Key Laboratory of Urban Pollutant Conversion, Department of Environmental Science and Engineering, University of Science and Technology of China, Hefei 230026, China

ARTICLE INFO

Article history:
Received 14 September 2022
Revised 19 November 2022
Accepted 29 November 2022
Available online 1 December 2022

Keywords:
Paired electrolysis
5-Hydroxymethylfurfural
2,5-Dihydroxymethylfuran
2,5-Furandicarboxylic acid
Co_3O_4

ABSTRACT

Production of value-added chemicals and fuels from biomass *via* electrochemical methods has been of emerging interest in light of the increasing environmental, economic, and political challenges. Paired electrolysis, with anodic oxidation and cathodic reduction reactions pairing in a single electrochemical cell, offers an effective way to produce desired products in both electrodes, thus achieving complete electron economy. In this work, an efficient 5-hydroxymethylfurfural (HMF) paired electrolysis system is developed over a self-supported ultrathin Co_3O_4 nanoarray electrocatalyst for simultaneous production of value-added 2,5-dihydroxymethylfuran (DHMF) and 2,5-furandicarboxylic acid (FDCA). The as-designed paired electrolysis cell achieves a high HMF conversion and DHMF/FDCA selectivity at both anode and cathode without external hydrogen and oxygen input. A near-quantitative yield (95.7%) of FDCA and 78.8% yield of DHMF can be achieved in the paired electrolysis system, with a total Faradaic efficiency of 127%. This work will open up new opportunities in designing efficient electrochemical devices to simultaneously produce building-block chemicals from biomass-derived molecules in both anode and cathode.

Producing chemicals and energy directly from biomass is an effective way to lessen the dependence on petroleum-based resources, which are on the verge of depletion. 5-Hydroxymethylfurfural (HMF), a representative furanic compound generated by acid-catalyzed dehydration of hexose sugars, is an important platform chemical linking raw biomass utilization and fine chemical production [1]. With two functionalities (−OH, C=O) attaching to a furan ring, HMF can be converted to several value-added chemicals *via* various redox processes [2]. One of its reduced derivatives, 2,5-dihydroxymethylfuran (DHMF), is an important precursor for the production of polyesters and polyurethane foams [3]. Its main oxidation product, 2,5-furandicarboxylic acid (FDCA), is a primary feedstock to produce polyethylene 2,5-furandicarboxylate, a renewable polymer alternative to petroleum-derived polyethylene terephthalate plastics [4]. Heterogeneous catalytic hydrogenation and oxidation of the HMF are the main methods for the production of DHMF and FDCA, respectively. However, these methods usually involve high-pressure H_2 or O_2, high temperature, and noble metal-based catalysts (*e.g.*, Au, Pt, Ru, and Pd) [3,4], which hinder their wide applications. Therefore, developing efficient methods for HMF conversion under mild conditions with cost-effective catalysts is highly desired.

The electrochemical method offers a promising way to replace the conventional heterogeneous catalytic system because of its advantages such as mild operating conditions, dispensing with noble-metal-based catalysts and easily controlled reaction process [5]. However, a typical electrochemical process usually involves two half-reactions occurring in pairs, yet many commercialized electrochemical production technologies utilize only one half-reaction to obtain desired products. For example, the cathodic HMF electrochemical reduction is usually paired with anodic water oxidation, which has sluggish kinetics and its main product oxygen gas is not valuable [6]. On the other hand, the anodic HMF oxidation is often paired with cathodic water reduction, in which less-value, flammable and combustible H_2 is a primary product [7].

Paired electrolysis, in which the anodic oxidation and cathodic reduction are paired in one single electrochemical cell, offers a robust way to obtain desired products in both electrodes and achieve complete electron economy [8]. Theoretically, the maximum electron efficiency of paired electrolysis could reach 200%.

* Corresponding author.
E-mail address: liuwujun@mail.ustc.edu.cn (W.-J. Liu).

https://doi.org/10.1016/j.cclet.2022.108034
1001-8417/

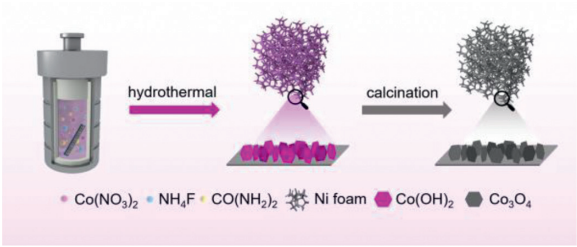

Fig. 1. The synthetic procedure of the Co_3O_4 NSA/Ni foam.

Moreover, the operation costs and equipment investments can be significantly reduced in the practical applications of the paired electrolysis technology by lowering the required reactor number and processing steps. For example, when the cathodic HMF reduction is paired with anodic HMF oxidation catalyzed by homogeneous 4-acetamido-2,2,6,6-tetramethylpiperidine-1-oxyl (4-ACT-TEMPO), DHMF and FDCA can be produced in the cathode and anode, respectively, with an overall electron efficiency of 187% [9]. However, the use of homogeneous 4-ACT-TEMPO will greatly increase the costs of downstream separation. Meanwhile, the cathodic HMF reduction is usually conducted under acidic conditions, in which acid-resistant catalysts are required [10], while the anodic HMF oxidation is usually performed under alkaline conditions with alkaline-resistant catalysts. Indeed, the Ag-based materials are reported as the most effective cathodic catalysts for HMF reduction [6,9], while the non-noble metal-based catalysts, such as Fe, Ni, and Co hydroxides have been exploited for anodic HMF oxidation [11]. Apart from the requirements of different electrocatalysts in anode and cathode, the chemical incompatibilities, mismatched optimal current densities for the two half-reactions, and crossover issues are also big challenges for the paired electrolysis of HMF.

Transition metal oxides with highly oxidized redox couples like $Co^{3+/4+}$, $Ni^{3+/4+}$, $Fe^{3+/4+}$, and $Mn^{3+/4+}$ have been known as active centers for many electro-oxidation reactions, such as oxygen evolution reaction (OER) and urea oxidation [12,13], while the metal oxides with reduced redox couples such as $Co^{2+/3+}$ and $Cu^{+/2+}$ are considered as the main active centers for some electro-reduction reactions, such as oxygen reduction reaction (ORR) and CO_2 reduction [14,15]. Among the numerous previously investigated transition metal oxides, Co_3O_4 should be a promising material for simultaneously catalyzing electro-oxidation and reduction reactions [16,17], as it can form a highly oxidized $Co^{3+/4+}$ redox couple under oxidation conditions, and a reduced $Co^{2+/3+}$ redox couple under reduction conditions.

Intending to develop an efficient paired electrolysis system to convert HMF into DHMF and FDCA, we synthesize a self-supported ultrathin Co_3O_4 nanoarray material and use it as a bifunctional electrocatalyst for both HMF oxidation and reduction. The self-supported electrode is an electrocatalytic material *in situ* grown on conductive support without any additional binder, conductive agent, or current collector [18]. The Co_3O_4 catalyst is closely contacting with the current collector, which is favorable to electron conduction. The high surface area, good electron conductivity and variable valence states endow it with a good performance in the electrocatalytic conversion of HMF.

The self-supported Co_3O_4 NSA electrocatalyst was synthesized *via* a two-step template-free approach (Fig. 1). In the hydrothermal process, urea was used to provide a basic condition to form $Co(OH)_2$ precursor and also a mineralizer to promote the crystallization of hexagonal nanosheet arrays [19]. The NH_4F could play an important role in regulating the growth of the $Co(OH)_2$ nanosheets on the Ni foam substrate [19]. Thereafter, the formed $Co(OH)_2$ was thermally converted into spinel Co_3O_4 nanoarray supported on the Ni foam, as described by a simple oxidation reaction as follows: $3Co(OH)_2 + 1/2O_2 \rightarrow Co_3O_4 + 3H_2O$. This method is facile and cost-effective to synthesize large-scale self-supported Co_3O_4 NSA electrodes with high robustness and conductivity, which is promising for practical electrode manufacture.

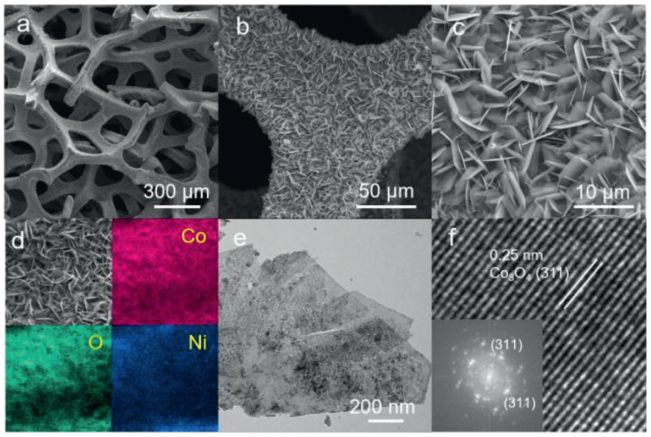

Fig. 2. (a-c) SEM images of the Co_3O_4 NSA/Ni foam with different magnifications; (d) EDS mapping, (e) TEM image, (f) HRTEM and SAED images of the Co_3O_4 NSA/Ni foam.

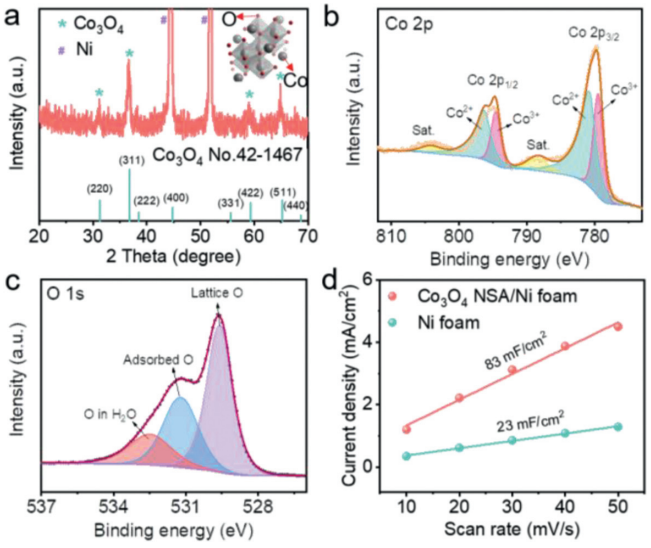

Fig. 3. (a) XRD pattern, high-resolution (b) Co 2p and (c) O 1s XPS spectra, and (d) double-layer capacitance of the Co_3O_4 NSA/Ni foam.

Scanning electron microscopy (SEM) images indicate that the Co_3O_4 grew uniformly on the Ni foam substrate in the form of vertical hexagonal nanosheets (Figs. 2a-c). Three elements of Co, O, and Ni were distributed uniformly with atomic concentrations of 42.7%, 37.4%, and 19.9% respectively, as characterized by the energy distributive spectroscopy (EDS) mapping (Fig. 2d and Fig. S1 in Supporting information). Transmission electron microscopy (TEM) images reveal that the thin sheets were composed of smaller particles (Fig. 2e). The selected area electron diffraction (SAED) (inset of Fig. 2f) displays a polycrystalline structure with (311) planes observed, which was also confirmed by the lattice spacings in high resolution (HRTEM) image (Fig. 2f).

Fig. 3a displays the X-ray diffraction (XRD) pattern of the ultrathin Co_3O_4 nanoarrays supported on the Ni foam. As the results show, except for the two typical diffraction peaks from the Ni foam substrate, other several well-defined diffraction peaks are observed at 2θ values of 31, 37, 59, and 65 degrees. All these diffraction peaks could be successfully indexed to (220), (311), (422) and (511)

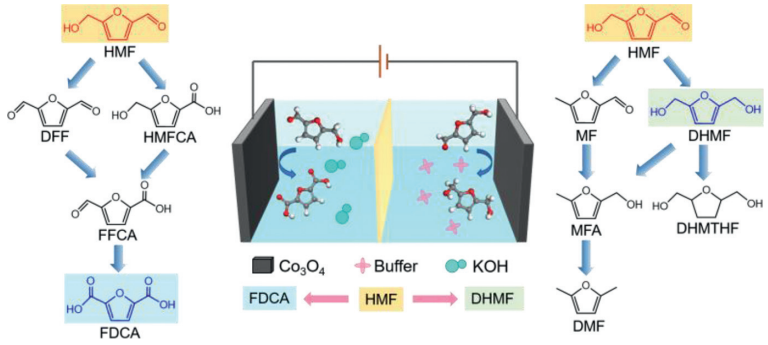

Scheme 1. Pathways of electrocatalytic oxidation (left) and hydrogenation (right) of HMF.

plane reflections of the spinel Co_3O_4 crystalline structure ((JCPDF No. 42-1467; space group: Fd3m) with the standard peaks indicated by the green lines shown in Fig. 3a. These results indicate that the Co_3O_4 NSA has uniformly grown on the surface of Ni foam substrate.

The X-ray photoelectron spectroscopy (XPS) survey spectrum (Fig. S2 in Supporting information) confirms that Co, O, and Ni were the main components of the electrode catalyst. The peaks at 796.5 and 780.9 eV were assigned to Co $2p_{1/2}$ and $2p_{3/2}$ signal of Co^{2+}, and the peaks at 794.6 eV and 779.6 eV belonged to Co $2p_{1/2}$ and $2p_{3/2}$ signal of Co^{3+} (Fig. 3b) [17]. The deconvoluted peaks of O 1s at 529.6 eV, 531.2 eV, and 532.5 eV indicate the existence of lattice O, adsorbed O, and O in H_2O (Fig. 3c) [20]. The Raman spectrum (Fig. S3 in Supporting information) further supports the existence of the Co_3O_4 phase, with the peaks at 654, 593, 504, 458, and 184 belonging to the A_{1g}, F_{2g}, F_{2g}, E_g, F_{2g} vibration modes of Co_3O_4 [21]. The EIS measurement was conducted to evaluate the charge transfer resistance at the interface of electrode and electrolyte. As the results showed (Fig. S4 in Supporting information), the semicircle reflecting the charge transfer resistance was small, no matter with or without HMF, indicating a fast charge transfer kinetics. This was probably related to the good electrical contact between the catalyst and the support. The surface area was characterized by N_2 adsorption-desorption tests and double-layer capacitance methods. The Brunauer-Emmett-Teller (BET) surface area was determined to be 6.84 m^2/g with a pore surface area of 8.06 m^2/g and a pore volume of 0.017 cm^3/g (Fig. S5 in Supporting information). The double-layer capacitance determined from cyclic voltammetry (CV) was 83 mF/cm^2 for the Co_3O_4 NSA/Ni foam (Fig. 3d and Fig. S6 in Supporting information), which was higher than that of the raw Ni foam (23 mF/cm^2), indicating a larger electrochemical active surface area (ECSA) could be obtained after growing Co_3O_4 on the Ni foam substrate.

Paired electrolysis is advantageous for maximizing electron efficiency and producing useful products in both chambers. We integrated the paired electrolysis of HMF in an electrolyzer using the Co_3O_4 NSA/Ni foam as electrodes on both sides. KOH and PBS were selected as electrolytes for anode and cathode reactions, respectively (Scheme 1 and Fig. S7 in Supporting information). The paired electrolysis was conducted by setting the cathodic potential at a constant value. Under −0.489 V *vs.* RHE, the current was as high as over 12 mA/cm^2 at the initial 20 min and declined from 20 min to 60 min. Later, the current kept at around 2 mA/cm^2 from 60 min to 120 min (Fig. 4a). Accordingly, the conversion of HMF reached about 80% in the initial 60 min and slowed down after 60 min. Overall, 95.7% yield of FDCA and 78.8% yield of DHMF were obtained in the anode and cathode, respectively (Figs. 4b and c). To examine the impact of voltage, the paired electrolysis was conducted under different potentials. The HMF conversion ratio increased with the increasing potential applied in both electrodes,

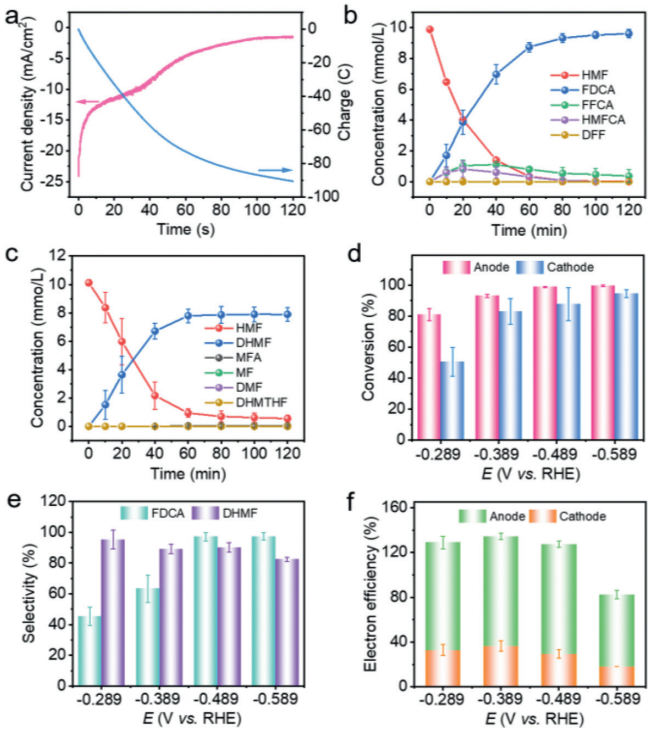

Fig. 4. (a) Current-time and charge-time plot in paired electrolysis at −0.489 V *vs.* RHE. (b) Concentration changes of HMF and its reduction products in cathode reaction, (c) concentration changes of HMF and its oxidation products in anodic reaction when cathode potential was set at −0.489 V *vs.* RHE. (d) HMF conversion ratios, (e) DHMF and FDCA selectivities, and (f) electron efficiencies on both sides at different potentials.

with a maximum value of 99.4% and 94.5% for the anode and cathode, respectively (Fig. 4d). The anodic selectivity increased with the increasing voltage and peaked at 97.3% at –0.589 V *vs.* RHE, while the cathodic selectivity decreased with the increasing voltage and peaked at 95.3% at −0.289 V *vs.* RHE (Fig. 4e). Since the electrons could be used in both anode and cathode, the total electron utilization efficiency for the paired electrolysis could be more than 100%. As shown in Fig. 4f, the total electron efficiency for the paired electrolysis from −0.289 V to −0.489 V was higher than 120%, while when the potential was shifted to −0.589 V, the Faradaic efficiency dropped down due to the enhancement of HER competition. Therefore the best performance was obtained at −0.489 V.

Five successive cycles of chronoamperometric tests were carried out to evaluate the durability of the Co_3O_4 NSA/Ni foam electrode in the paired HMF electrolysis. In the cathode (Fig. 5a), the HMF conversion ratio slightly decreased from 93% to about 89% after 5 cycles, while the corresponding DHMF selectivity kept almost over

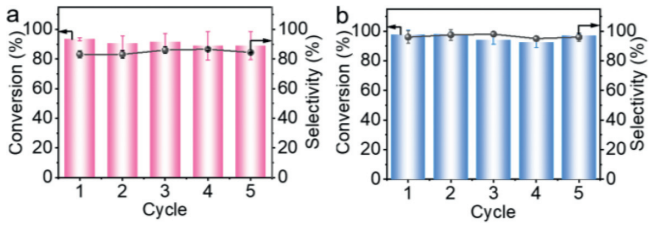

Fig. 5. HMF conversion ratios and product selectivities on (a) cathode and (b) anode in five cycles.

80%. Meanwhile, in the anode (Fig. 5b), the HMF conversion and its selectivity to FDCA were maintained at over 95% in the five cycles.

The cycled Co_3O_4 NSA electrodes were then characterized with SEM and HRTEM. As shown in Fig. S8 (Supporting information), the anodic and cathodic Co_3O_4 NSA still kept their nanosheet morphology after five cycles, but some small particles were observed in the cathodic Co_3O_4 NSA. The changes in crystal phase and electronic structure before and after use were further analyzed with XRD and XPS. For cathodic catalyst, the XRD result (Fig. S9c in Supporting information) exhibits a weakened crystallinity of Co_3O_4, and XPS analysis (Figs. S9a and b in Supporting information) shows a reduction of surface cobalt state, together with a decrease in lattice oxygen and an increase in adsorbed oxygen. These results lead to the conclusion that Co_3O_4 experienced a reduction during reaction in the cathode. As for the anodic catalyst, the morphology was kept unchanged after five cycles (Fig. S8), and its XRD (Fig. S9c) and XPS results (Figs. S9a and b) also suggest no prominent change compared with the original Co_3O_4, indicating that Co_3O_4 was stable under the oxidative and alkaline conditions, which is beneficial for the long-term run. The above-paired electrolysis system was compared with previously reported work involving paired electrolysis of HMF (Table S1 in Supporting information). Our work is advantageous in the development of a bifunctional non-noble catalyst, a mild reaction condition and a satisfactory product yield.

The mechanism for the electro-oxidation and hydrogenation of HMF over Co_3O_4 NSA was investigated. As for the anodic part, there were two possible mechanisms for the electrocatalytic oxidation of HMF, namely, direct oxidation and indirect oxidation [11]. In direct oxidation, the valence state of the catalyst keeps unchanged throughout the reaction, and the potential is used to directly drive the oxidation of substrates. In indirect oxidation, the potential does not directly drive the oxidation of the substrate but changes the chemical state of the catalyst, and the catalyst serves as a redox mediator to oxidize the substrate [11]. In this work, an indirect oxidation mechanism was preferred due to the following phenomenon: First, in the CV tests, the addition of HMF enhanced the oxidation peak of Co^{3+}, which is possibly due to the generated Co^{4+} being quickly reduced by HMF, thus accelerating the oxidation process from Co^{3+} to Co^{4+} (Fig. S10a in Supporting information). The electron transfer between the electrode, Co_3O_4, and HMF was fast enough thus making the HMF diffusion become the rate-limiting step, which is the reason for the linear relationship between HMF concentration and peak current (Figs. S10b and c in Supporting information). We further conducted multi-potential measurements to verify our assumption. As shown in Fig. S10d (Supporting information), the Co_3O_4 was first oxidized at 1.42 V to enrich the high-valence Co^{4+}. When the potential was changed to an open circuit potential (OCP), a reduction current appeared, indicating a discharge from Co^{4+} to Co^{3+}. However, when 50 mmol/L HMF was injected into the electrolyte before switching to OCP, the reduction current became not evident, suggesting the Co^{4+} was consumed by the injected HMF [12]. These results indicate that the oxidation of HMF over Co_3O_4 at 1.42 V is an indirect oxidation process [22].

From the above results, we can infer that a valence state circulation of cobalt in Co_3O_4 existed in the catalytic oxidation process. (Fig. 6a) In detail, Co^{3+} was first oxidized into Co^{4+} under the positive potential (reaction 1), and HMF was hydrated in the presence of OH^- (reaction 2). The high-valence Co^{4+} could directly seize proton and electron from the hydrated aldehyde group, which led to the generation of HMFCA and Co^{3+} (reaction 3). Co^{4+} could continue to oxidize the hydroxy group into aldehyde group, which generated FFCA (reaction 4). Once the aldehyde group was hydrated (reaction 5), FFCA could be further oxidized into FDCA by Co^{4+} (reaction 6). The circulation of Co^{3+} and Co^{4+} continued in the oxidation process. OH^- promoted the oxidation of Co_3O_4 into CoO_2 and the hydration of HMF, which largely accelerated the reaction kinetics.

$$Co_3O_4 - 6e + 6OH^- \longrightarrow 4.5CoO_2 + 6H_2O \quad (1)$$

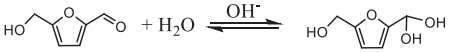

(2)

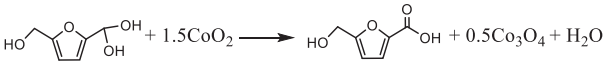

(3)

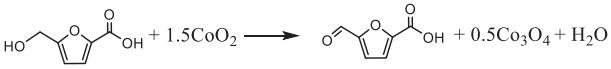

(4)

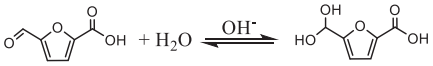

(5)

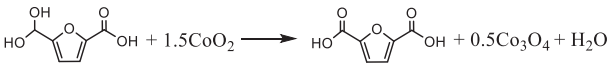

(6)

As for the cathodic HMF reduction, in CV results (Fig. S11a in Supporting information), the reduction of Co^{3+} to Co^{2+} seems quenched in the presence of HMF. However, the valence state of cobalt transformed into +2 after the reaction, as shown in Fig. S9a. Thus, we attribute the reduction peak at −0.15 V to the reduction of Co^{3+} to Co^{2+}, and the peak at −0.4 V should be the one-electron reduction of HMF. Besides, the ECH process only proceeded in PBS electrolyte rather than the non-buffered Na_2SO_4 electrolyte (Fig. S11b in Supporting information), which indicates that PBS rather than water was the proton donor. Considering that HER reaction was accompanied by the ECH process, which suggests adsorbed hydrogen (H*) must exist on the electrode [23], we propose a two-step reduction mechanism (Fig. 6b). That is, Co_3O_4 was first reduced to a lower-valence $Co(OH)_2$ (reaction 7), and H* was formed at the surface of $Co(OH)_2$ (reaction 8). The adsorbed HMF could be reduced to a ketyl radical through proton-coupled electron transfer (PCET, reaction 9), which could be further reduced to DHMF by H* or another (PCET) process (reaction 10).

$$Co_3O_4 + 2e + 2H_2PO_4^- + 2H_2O \longrightarrow 3Co(OH)_2 + 2HPO_4^{2-} \quad (7)$$

$$H_2PO_4^- + e \longrightarrow H^* + HPO_4^{2-} \quad (8)$$

(9)

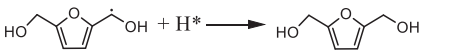

(10)

In summary, this work demonstrates that HMF could be efficiently converted into two important biobased polymer precursors, DHMF and FDCA, in a paired electrolyzer with a single non-noble metal-based catalyst. The Co_3O_4 NSA/Ni foam could work as a bifunctional catalyst for simultaneous electrocatalytic oxidation and hydrogenation of HMF. Under the optimized conditions, 78.8% yield of DHMF and 95.7% of FDCA were obtained along with an overall Faradaic efficiency of 127.0%. This work shows the potential ad-

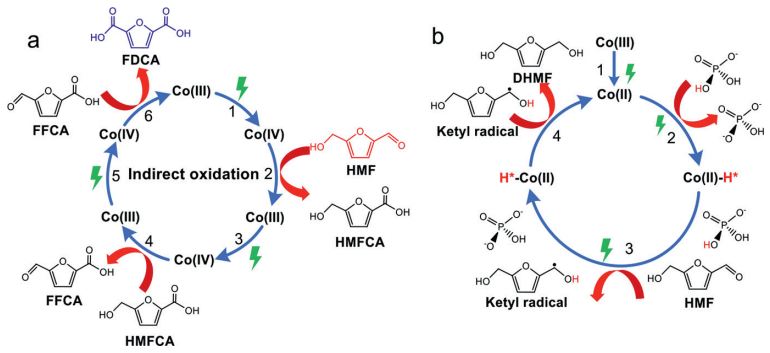

Fig. 6. The proposed mechanism for (a) electrocatalytic oxidation and (b) hydrogenation of HMF over Co_3O_4 NSA electrocatalyst.

vantages of paired electrolysis for achieving efficient utilization of electrons for producing valuable chemicals.

Declaration of competing interest

The authors declare that they have no known competing financial interests or personal relationships that could have appeared to influence the work reported in this paper.

Acknowledgments

The authors gratefully acknowledge the support from the National Natural Science Foundation of China (Nos. 22122608, 21976170, U20A20325 and 51821006), the Fundamental Research Funds for the Central Universities (Nos. WK3530000009, YD2400002001), and the Program for Changjiang Scholars and Innovative Research Team in University of the Ministry of Education of China.

Supplementary materials

Supplementary material associated with this article can be found, in the online version, at doi:10.1016/j.cclet.2022.108034.

References

[1] Q. Hou, X. Qi, M. Zhen, et al., Green Chem. 23 (2021) 119–231.
[2] X. Kong, Y.F. Zhu, Z. Fang, et al., Green Chem. 20 (2018) 3657–3682.
[3] L. Hu, J. Xu, S. Zhou, et al., ACS Catal. 8 (2018) 2959–2980.
[4] M. Sajid, X.B. Zhao, D.H. Liu, Green Chem. 20 (2018) 5427–5453.
[5] S.A. Akhade, N. Singh, O.Y. Gutier, et al., Chem. Rev. 120 (2020) 11370–11419.
[6] J.J. Roylance, T.W. Kim, K.S. Choi, ACS Catal. 6 (2016) 1840–1847.
[7] B. You, X. Liu, X. Liu, et al., ACS Catal. 7 (2017) 4564–4570.
[8] R.S. Sherbo, R.S. Delima, V.A. Chiykowski, et al., Nat. Catal. 1 (2018) 501–507.
[9] X.H. Chadderdon, D.J. Chadderdon, T. Pfennig, et al., Green Chem. 21 (2019) 6210–6219.
[10] P. Zhou, L.B. Li, V.S.S. Mosali, et al., Angew. Chem. Int. Ed. 61 (2022) e202117809.
[11] Y. Yang, T. Mu, Green Chem. 23 (2021) 4228–4254.
[12] W. Chen, C. Xie, Y.Y. Wang, et al., Chem. 6 (2020) 2974–2993.
[13] N.T. Suen, S.F. Hung, Q. Quan, et al., Chem. Soc. Rev. 46 (2017) 337–365.
[14] S. Nitopi, E. Bertheussen, S.B. Scott, et al., Chem. Rev. 119 (2019) 7610–7672.
[15] S. Gao, Y. Lin, X. Jiao, et al., Nature 529 (2016) 68–71.
[16] T. Kosmala, L. Calvillo, S. Agnoli, et al., ACS Catal. 8 (2018) 2343–2352.
[17] Z. Wang, H. Liu, R. Ge, et al., ACS Catal. 8 (2018) 2236–2241.
[18] H.Y. Yang, M. Driess, P.W. Menezes, Adv. Energy Mater. 11 (2021) 2102074.
[19] J. Jiang, J.P. Liu, X.T. Huang, et al., Cryst. Growth Des. 10 (2009) 70–75.
[20] S. Xiong, J.S. Chen, X.W. Lou, et al., Adv. Funct. Mater. 22 (2012) 861–871.
[21] V.G. Hadjiev, M.N. Iliev, I.V. Vergilov, J. Phys. Chem. C: Solid State Phys. 21 (1988) L199–L201.
[22] Y. Lu, T. Liu, Y.C. Huang, et al., ACS Catal. 12 (2022) 4242–4251.
[23] N. Dubouis, A. Grimaud, Chem. Sci. 10 (2019) 9165–9181.